

PHYSICAL REVIEW B

CONDENSED MATTER

THIRD SERIES, VOLUME 38, NUMBER 7

1 SEPTEMBER 1988

Structure of a $(\text{RhCl}_6)^{4-}$ defect in AgCl

M. T. Olm

Corporate Research Laboratories, Eastman Kodak Company, Rochester, New York 14650

J. R. Niklas and J. M. Spaeth

University of Paderborn, Paderborn, West Germany

M. C. R. Symons

University of Leicester, Leicester, England

(Received 1 February 1988)

The structure of the primary rhodium defect in rhodium-doped AgCl was determined by EPR and electron-nuclear double-resonance technique spectroscopies. The substitutional and orthorhombic Rh^{2+} complex, $(\text{RhCl}_6)^{4-}$, was elongated along a [100] axis with a silver ion vacancy in a next-nearest-neighbor position in the plane perpendicular to the elongation axis. The large superhyperfine interactions measured for the first-shell chloride ions and the fourth-shell silver ions along the elongation axis suggest that the complex was stabilized by covalent interactions. The structural model deduced from these experiments provided an explanation for the dynamic behavior of the complex which was observed above ~ 80 K.

INTRODUCTION

Trivalent transition-metal ions can be incorporated into silver halide melt-grown single crystals by addition to the melt, and into powders and photographic emulsions by coprecipitation from aqueous solution. The majority of such addenda occupy substitutional positions on the cation sublattice and act as photoelectron traps. They can have a significant effect on the performance of the silver halides as photographic materials.¹⁻⁴

In the silver halides, aliovalent impurity cations are generally associated with charge-compensating silver ion vacancies. It has been found experimentally that the trapping behaviors of impurity-defect complexes are very sensitive to the number and arrangement of vacancies.³ While EPR spectroscopy has proven to be a valuable tool in studying the photobehavior of such complexes, the resonances observed are always broadened by superhyperfine (shf) interactions with the many surrounding magnetic nuclei. Superhyperfine structure is usually only resolved for either axial or equatorial first-shell halide ions, so that the structure of the impurity-vacancy complex must be inferred from the symmetry of the g matrix. More-detailed structural information should be obtainable from electron-nuclear double-resonance technique (ENDOR) spectroscopic studies.

Rhodium(III), because of its properties as a long-lived, deep electron trap, is widely used as a dopant in some photographic products to increase contrast. The diamagnetic

ion, Rh^{3+} , is incorporated in crystals grown in a halogen environment. The $\text{Rh}^{2+}(d^7)$ species can be produced by photolysis or by annealing in air above 300°C or *in vacuo*.⁴

The rhodium(II) species in AgCl has been studied previously by EPR.^{5,6} At temperatures less than 110 K, an axially symmetric spectrum was reported, with $g_{\perp} > g_{\parallel}$, and shf splittings from two equivalent chloride ions. Above 160 K, this reversibly converted to a spectrum with $g_{\parallel} > g_{\perp}$ showing no resolved shf interactions. At temperatures above 200 K, this spectrum began to disappear, reversibly converting to a single, broad isotropic line. Only this line was observed above 350 K. These spectra were incorrectly assigned to Jahn-Teller distorted $(\text{RhCl}_6)^{6-}$ complexes (Rh^0, d^9). Accordingly, it was deduced that the unpaired electron occupied a compressed d_{z^2} ground state below 110 K, an elongated $d_{x^2-y^2}$ ground state above 160 K, with a dynamic distortion between these two states occurring above 200 K.⁵ No explanation was given for the observed distortion or the change in the ground state. On the basis of later EPR studies of the $(\text{RhBr}_6)^{4-}$ complex in AgBr,⁴ the complexes in AgCl were reassigned to the d^7 , $(\text{RhCl}_6)^{4-}$, ion,⁶ which was, therefore, elongated below 110 K, compressed above 160 K and undergoing a dynamic distortion above 200 K. For the elongated Rh^{2+} complex observed below 110 K in AgBr, the source of distortion was attributed to the presence of a charge-compensating silver ion vacancy along the elongation axis. The existence of such a structure was puzzling, however,

since a contraction rather than an elongation was observed along the dopant-vacancy axis for several other dopant-vacancy complexes for which structures had been deduced from EPR data.^{1,2}

The present EPR and ENDOR study was undertaken to obtain further details of the structure of the Rh^{2+} -vacancy complex in AgCl . Resolved hyperfine and shf interactions of the unpaired electron with some of the six chlorine ions surrounding the Rh^{2+} ion, as well as with the rhodium ion and two fourth shell silver ions, were observed. This has led to a new structural model for the center, and an explanation for the reported changes in the EPR spectrum based upon the dynamical behavior of the low-temperature complex.

EXPERIMENT

Rhodium-doped single crystals were grown from ultrapure AgCl using the dopant salt $\text{Na}_3\text{RhCl}_6 \cdot \text{H}_2\text{O}$. Crystals were grown under chlorine by the Bridgman method, aligned by the standard x-ray back-reflection technique, and cut into cubes with either [100] or [110] axes perpendicular to the cube faces. Crystals with nominal dopant levels of 50, 200, and 1000 mppm were studied. The crystals ranged in color from light orange to dark red. Crystals from the latter boules are referred to below as heavily doped, and from the 50- and 200-mppm boules as lightly doped. The Rh^{2+} species was produced by annealing the crystals at 300 °C in air. In this way, a stronger EPR signal was produced than could be obtained by photolysis. The species could not be produced by annealing in chlorine.

Most ENDOR measurements were done with a computer-controlled ENDOR spectrometer at the University of Paderborn.⁷ Some measurements were made using a Bruker 200D EPR-ENDOR spectrometer and Oxford Instruments helium cryostat. Some EPR measurements were performed using a Varian Q-band spectrometer at 77 K.

RESULTS

EPR measurements

Intense EPR spectra were obtained from both lightly doped and heavily doped Rh^{3+} - AgCl single crystals, which had been heat treated as described above. Signals from primary and secondary centers were observed. The spectrum of the primary species and its temperature behavior were essentially the same as previously reported.^{5,6}

Resonances from the secondary species were observed in all crystals and were relatively more intense in lightly doped crystals. These signals are just visible in the EPR spectrum for $B_0 \parallel [100]$ of the heavily doped crystal in Figs. 1(a) and 1(e). Despite the overlap of the EPR signals from the primary and secondary species, it was determined using the double ENDOR technique described below that all of the ENDOR resonances described in this paper were attributable to the primary species. The secondary species will not be discussed further here.

For the primary Rh^{2+} complex, a different EPR spec-

trum was observed in each of three temperature ranges. These signals could be reversibly interconverted by varying the temperature. The predominant form of the primary complex in each of these temperature ranges is referred to below as the low-temperature (LT) form, the high-temperature (HT) form, and the isotropic form, respectively (Fig. 1). The temperatures of transition between the three forms and the degree of spectral resolution for the HT and isotropic forms were very dependent on dopant concentration. For the lightly doped samples, the LT, HT, and isotropic spectra predominated, respectively, below 80 K, above 110 K, and above 280 K. For heavily doped samples, well-resolved shf structure for the HT and isotropic forms were not observed at any temperature. In these samples, distinct spectra from the HT and isotropic forms were observed about 50 K higher than in the lightly doped samples. The relationship between dopant level and temperature behavior probably accounts for the differences between our transition temperatures and those reported by Wilkens, DeGraag, and Helle.⁵

The EPR spectrum of the LT form of the primary Rh^{2+} complex is shown in Fig. 1(a). EPR angular rotation studies in the (100) and (110) planes revealed that for the LT form, the principal values of the g matrix were parallel to the [100] crystal axes and that the g matrix

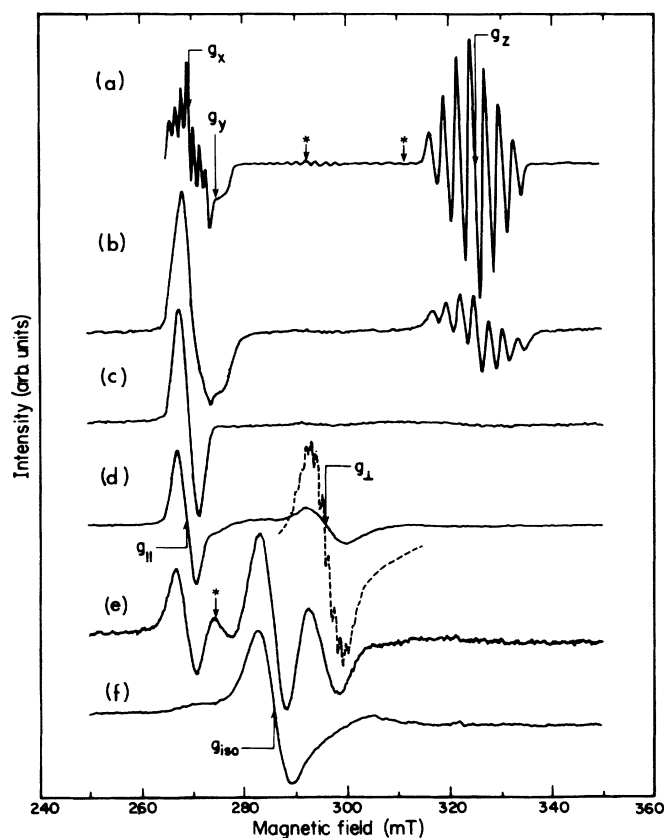


FIG. 1. EPR spectrum of the primary $(\text{RhCl}_6)^{4-}$ complex in a heavily doped AgCl single crystal, measured at (a) 20 K, (b) 90 K, (c) 130 K, (d) 180 K, (e) 300 K, and (f) 400 K, with B_0 along (100). The inset spectrum (dashed line) in (d) is from a lightly-doped AgCl single crystal. The asterisks denote resonances from the secondary rhodium complex.

had orthorhombic symmetry, not axial symmetry as previously reported.^{5,6} The resolution and relative intensities of the symmetry-related g components were very dependent on temperature, which could explain the earlier failures to note the orthorhombic character of the g matrix. For simplicity, the principal symmetry-related g components of the LT form will be referred to as g_x , g_y , and g_z , where the subscripts x , y , and z refer to the Rh^{2+} complex axes as labeled in Fig. 2. Thus, g_z is parallel to $[100]$ and to the elongation axis of the Rh^{2+} complex and g_x and g_y are in the equatorial plane, with g_x parallel to the Rh^{2+} next-nearest-neighbor (NNN) vacancy axis. These assignments will be justified below.

The data for the LT form could be described by the first-order solution to the general spin Hamiltonian given below, with the selection rules $\Delta m_S = \pm 1$, $\Delta m_I = 0$, for the EPR experiment:

$$\mathbf{H} = \mu_B \mathbf{B}_0 \cdot \mathbf{g}_e \cdot \mathbf{S} + \sum_{i=1}^n (\mathbf{I}_i \cdot \mathbf{A}_i \cdot \mathbf{S} - g_{n_i} \mu_{n_i} \mathbf{B}_0 + \mathbf{I}_i \cdot \mathbf{Q}_i \cdot \mathbf{I}_i). \quad (1)$$

The symbols have their usual meaning^{8,9} and S was assumed to equal $\frac{1}{2}$, which was confirmed by the ENDOR measurements. The observed EPR spectra indicated that $n = 2$, $I = \frac{3}{2}$, describing a superhyperfine (shf) interaction with two equivalent chloride nuclei.

The dynamic behavior of the primary Rh^{2+} complex is illustrated by Fig. 1. As the temperature was raised above 80 K, the resolved hyperfine structure on the g_x and g_y features began to disappear and the g_z feature became weaker relative to the g_x and g_y features [Fig. 1(b)]. As the temperature was raised still further, the g_y and g_z components disappeared, leaving a symmetric line at $g = 2.435$, close to the g value of 2.426 measured at low temperature for g_x . Further annealing produced the spectrum of the HT form, shown in Fig. 1(d), composed of lines with g values of 2.435 and 2.211. Rotation studies

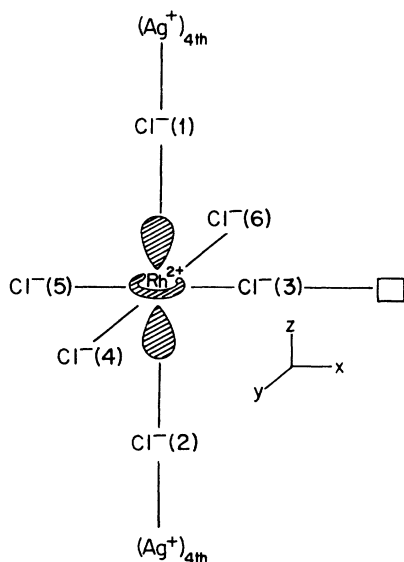


FIG. 2. Model of the low-temperature, primary rhodium complex in AgCl .

TABLE I. g values of the low-temperature, high-temperature, and isotropic forms of the primary Rh^{2+} species in AgCl .

Type of distortion	g components ^a		
	x	y	z
Static elongation (low-temperature form)	2.426	2.395	2.011
Dynamic two dimensional (high-temperature form)	2.435	2.211	2.211
Dynamic three dimensional (isotropic form)	2.291	2.291	2.291

^a ± 0.002 .

showed that $g = 2.435$ was a principal g value, which rotated as a parallel g feature, and that the line at $g = 2.211$ rotated as a perpendicular g feature. The symmetry-related principal g components of the high-temperature form will be referred to as g_{\parallel} and g_{\perp} . These were parallel to the cubic crystal axes.

At approximately 210 K, an isotropic EPR signal appeared at a g value of 2.291 [Fig. 1(e)]. As the temperature was raised, this line grew in intensity, while the g_{\parallel} and g_{\perp} components for the HT form broadened and moved towards the isotropic line. At 400 K, the highest temperature attainable with the EPR cavity used, the isotropic species was the only resolved line present, with a small amount of spectral anisotropy apparent in the wings [Fig. 1(f)].

The principal g values of the LT form, the HT form, and the isotropic form of the primary Rh^{2+} complex are listed in Table I. It can be seen that g_x from the LT form was very close to g_{\parallel} from the HT form. Additionally, $[\frac{1}{2}(g_x^2 + g_z^2)]^{1/2}$ from the LT form was the same as g_{\perp} from the HT form.

ENDOR measurements

The relaxation characteristics of the rhodium complex in AgCl required that all ENDOR measurements be done at approximately 30 K, and thus only the LT form of the primary species was examined. An angular-rotation study was performed by taking an ENDOR spectrum every two degrees over a 50° interval in a (100) plane, using the magnetic field B_0 to select one or two of the three symmetry-related orientations of the $(\text{RhCl}_6)^{4-}$ complex. Due to the large g anisotropy, ENDOR spectra could be obtained independently from those complexes with their g_z axes parallel to B_0 and from those with g_z perpendicular to B_0 .

The presentation of the ENDOR data is facilitated by referring to the model of the $(\text{RhCl}_6)^{4-}$ defect shown in Fig. 2. The largest shf interaction observed by ENDOR resulted from the two first-shell chlorines along the z axis (axial chloride ions), which also gave rise to the seven-line g_z EPR feature [Fig. 1(a)]. Additionally, interactions with the fourth-shell silver ions along the z axis (axial silver ions) were measured. Some interactions with the first-shell chloride ions in the x - y plane (equatorial chloride ions) were also observed.

A section of the ENDOR spectrum, measured while saturating the g_z component of the EPR spectrum shown in Fig. 1(a), that is, selecting the centers with their g_z axes parallel to \mathbf{B}_0 , is shown in Fig. 3. The frequency range is that where the ENDOR lines corresponding to the resolved EPR septet would be expected. The lines can be assigned to transitions of the ^{35}Cl and ^{37}Cl isotopes based on relative intensities and separations. The positions of the lines, treating $\text{Cl}^-(1)$ and $\text{Cl}^-(2)$ as independent nuclei, are given by the first-order solution of the Hamiltonian in Eq. (1), with the selection rules $\Delta m_S = 0$, $\Delta m_I = \pm 1$:

$$\Delta E_{\text{ENDOR}} = |Am_s - g_N\mu_N B_0 + m_q W_q|. \quad (2)$$

The variable m_q is given by $\frac{1}{2}(m_I + m_I')$ where m_I and m_I' are the chlorine nuclear spin states involved in the transition. A is the shf interaction parameter. W_q is the quadrupole interaction parameter. Thus, for each isotope, the two "hyperfine" lines, marked $m_q = 0$ in Fig. 3, are split into three by a quadrupole interaction at the chlorine nucleus. To first order, the positions of the hyperfine lines are not influenced by the quadrupole transition.

The hyperfine lines ($m_q = 0$) of the ^{35}Cl ENDOR transitions in Fig. 3 were further split by an amount given approximately by $a^2/g_e\mu_B B_0$, where a is the isotropic hyperfine constant for the axial ^{35}Cl 's. Such a splitting was not observed on the ^{37}Cl ENDOR transitions. This indicates that the splittings resulted from second-order, indirect spin-spin coupling between equivalent chloride ions.^{8,10} Since the chloride isotope pairs ^{35}Cl - ^{35}Cl , ^{35}Cl - ^{37}Cl , and ^{37}Cl - ^{37}Cl , occur in the ratio of 9:6:1, the largest contribution to the ^{35}Cl ENDOR transitions would be from equivalent chlorine nuclei in ^{35}Cl - ^{35}Cl pairs. Second-order splittings due to indirect coupling of inequivalent chloride ions (i.e., ^{35}Cl - ^{37}Cl pairs) would be less than the ENDOR linewidths. Therefore, the splittings of the ^{37}Cl ENDOR transitions were not detected.

Using the technique of ENDOR-induced EPR, which

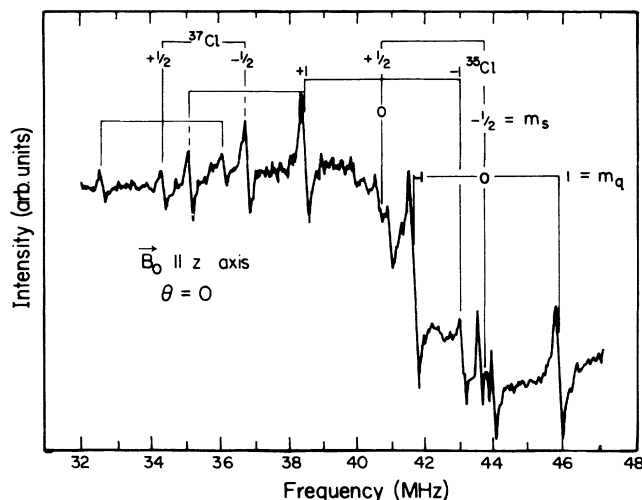


FIG. 3. ENDOR spectrum of transitions from axial chloride ions in primary rhodium complexes with g_z parallel to \mathbf{B}_0 (measured with $\mathbf{B}_0 \parallel [100]$), showing the second-order splittings on the ^{35}Cl hyperfine lines due to equivalent nuclei.

allowed the correlation of EPR and ENDOR transitions involving the same axial chloride ion nuclear-spin state,¹¹ it was established that the quadrupole interaction W_q and the shf interaction A had opposite signs.

Double ENDOR experiments were used as an aid in assigning ENDOR transitions, since it was difficult to track individual ENDOR lines once the field was rotated more than 20° from the g_z axis of the complex, mainly due to the second-order splittings of the ENDOR lines. In the double ENDOR experiments, a second rf emitter is used to excite an ENDOR line belonging to a particular complex, while the first rf source is swept, as usual, through the frequency range of interest. In the double ENDOR spectrum only transitions belonging to the complex excited by the second rf source appear. Thus, as a result of the relative abundances of chlorine isotope pairs, transitions from ^{35}Cl nuclei in ^{35}Cl - ^{37}Cl pairs, which showed no second-order splittings, could be observed separately in a double ENDOR experiment in which ^{37}Cl transitions were pumped.

Using an iterative simulation and fitting process for the analysis of the ENDOR angular rotation patterns, the spin Hamiltonian was diagonalized and the interaction parameters were extracted.⁷ The spin Hamiltonian used was that shown in Eq. (1), with the simplifying assumption that each nucleus acted independently. The results are given in terms of the isotropic hyperfine (hf) and superhyperfine interaction, represented by a , and the anisotropic hf or shf interaction, represented by b and b' , which are related to the principal hf or shf matrix by

$$\begin{aligned} A_{11} &= a - b + b', \\ A_{22} &= a - b - b', \\ A_{33} &= a + 2b. \end{aligned} \quad (3)$$

The parameter b' denotes the deviation from axial symmetry. Similarly, the quadrupole interaction constant q is related to the principal values of the quadrupole tensor by

$$\begin{aligned} Q_{11} &= -q + q', \\ Q_{22} &= -q - q', \\ Q_{33} &= 2q. \end{aligned} \quad (4)$$

q' is the asymmetry parameter and is zero for axial symmetry. The measured quadrupole splitting is given by

$$W_q = 3 \left[q(3 \cos^2 \theta - 1) + \frac{q'}{\sin^2 \theta \cos^2 \theta} \right]. \quad (5)$$

The quadrupole interaction constant q is related to the electric field gradient $\partial^2 V / \partial Z^2$ at the nucleus by

$$q = \frac{eQ}{4I(2I-1)} \frac{\partial^2 V}{\partial Z^2} = \frac{Q_{33}}{2}. \quad (6)$$

The angular ENDOR data for the axial chloride ions were fitted to an orthorhombic hf matrix with principal axes parallel to the $\langle 100 \rangle$ crystal axes. The shf and quadrupole data for the axial chloride ions are collected in Table II. By simulating the g_x region of the $[100]$ EPR spectrum (Fig. 4) it was determined that the hyperfine

TABLE II. Hyperfine constants for ligands of the primary rhodium complex in AgCl (in MHz). The uncertainty in the magnitude of these constants is one or two units in the last digit.

	a/h	b/h	b'/h	q/h	q'/h
$^{35}\text{Cl}_{1,2}$	54.0	11.8	2.6	-0.4	-0.14
$^{109}\text{Ag}_{4\text{th}}$	10.7	1.0			
^{103}Rh	7.0	1.0	0.54		
$^{35}\text{Cl}_{4,6}$		$A_{33} \approx 25$			

principal direction corresponding to the smallest principal value, A_{11} , was parallel to x . It was obvious from the parallel region of the EPR spectrum that A_{33} was along z ; thus, A_{22} must be along y .

Figure 5 is a section of the ENDOR angular dependence in the frequency range 2–6 MHz for the rotation of B_0 in the xy plane. It clearly shows the ^{103}Rh transitions, whose line separations were consistent with the value of the ^{103}Rh magnetic moment. Also shown are four transitions from the axial fourth-shell Ag^+ ions. The relative positions and intensities of the four lines are those predicted from the ratios of the nuclear moments and the natural abundances of the two silver isotopes, ^{109}Ag and ^{107}Ag . For both rhodium and silver nuclei, all natural isotopes have a nuclear spin of $\frac{1}{2}$, so no quadrupole splitting was observed. For both nuclei, the principal shf values were measured along the $[100]$ cubic axes. The rhodium transitions exhibited a very orthorhombic angular dependence (b' large) while the silver transitions were axial, with a completely isotropic interaction in the equatorial plane. This angular behavior justifies the assignment of these silver transitions to nuclei along the z axis (Fig. 2). The Hamiltonian parameters for the central rhodium ion and the fourth-shell axial Ag^+ ions were fitted as described above and are collected in Table II. Some of the calculat-

ed fits are shown in Fig. 5. For both nuclei the largest shf interaction A_{33} was measured along z . For the rhodium nucleus it was assumed that as for the axial chloride ions the smallest shf interaction A_{11} was along x .

Also evident in Fig. 5 are a number of unassigned ENDOR transitions showing strong angular dependences. Those close to the axial fourth-shell silver transitions, between 3.5 and 6.0 MHz, are most likely from fourth-shell silver ions along the g_z axis which are perturbed from axial symmetry possibly by some distant defect. The relative intensities of the resonance from the fourth-shell silver ions along the z axis with axial symmetry and those with nonaxial symmetry can be seen in the ENDOR spectrum in Fig. 6. This ENDOR spectrum, corresponding to $\theta = 42^\circ$ in Fig. 5, is from those complexes with their g_z axes perpendicular to B_0 and with B_0 approximately halfway between g_x and g_y . In the xz and yz planes, the angular dependences of the nonaxial silver lines paralleled those of the axial fourth-shell silvers. It was only in the equatorial plane that a major difference in angular dependence pattern was observed. The difference in the shf interaction parameters compared to the unperturbed complex was only 1.5%. Double ENDOR experiments showed that the low-symmetry fourth-shell silver lines originated from the same complexes which gave rise to the axial chlorine ENDOR transitions, the rhodium transitions, and the axial fourth-shell silver transitions.

These observations can be explained if it is assumed that some of the primary rhodium complexes were perturbed by a distant defect or impurity. For any such perturbation not in the equatorial plane, one of the axial fourth-shell silver ions would be closer and more affected by its presence. It would be possible therefore for a complex to have one fourth-shell silver along the z axis with

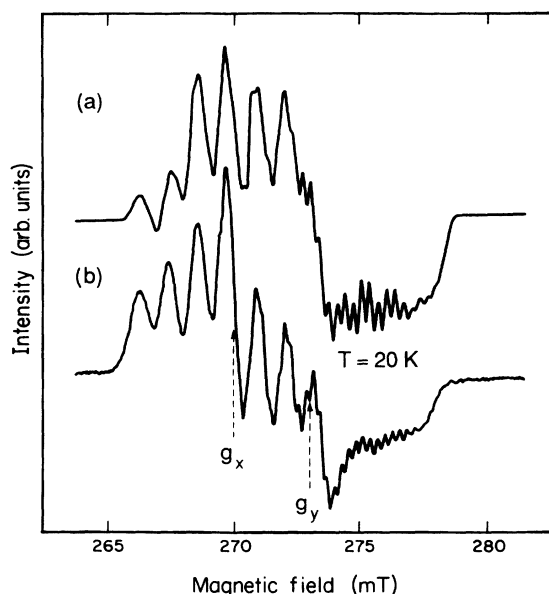


FIG. 4. Simulated (a) and experimental (b) g_x and g_y components of the $[100]$ EPR spectrum of the primary $(\text{RhCl}_6)^{4-}$ complex.

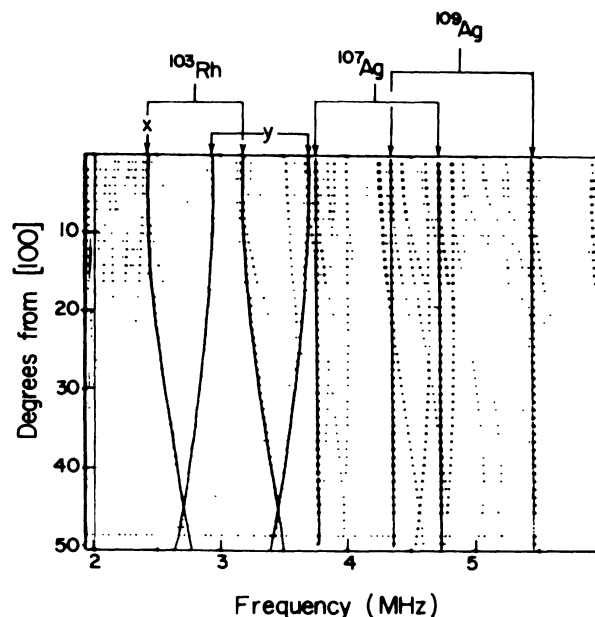


FIG. 5. Angular rotation plot of Rh^{2+} and fourth-shell silver ENDOR transitions in the (100) plane perpendicular to g_z . The dot size is proportional to signal intensity.

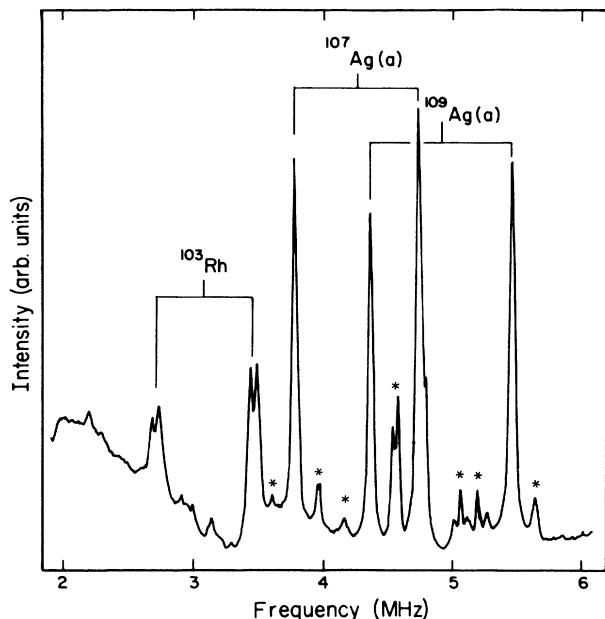


FIG. 6. ENDOR spectrum, measured with B_0 perpendicular to g_z and approximately along [110], showing the relative intensities of the transitions from Rh^{2+} and from the fourth-shell silver ions with axial [Ag(a)] and with nonaxial (*) symmetry.

axial symmetry and one with lower symmetry. The majority of complexes, however, would be completely unperturbed by distant defects, and ENDOR transitions from their equivalent axial chloride ions would exhibit the observed second-order splittings mentioned above. Alternatively, the axial chloride ions of the perturbed complexes might be considered equivalent, depending on the distance and influence of the perturbing defect.

The measurement and assignment of the ENDOR transitions from the equatorial chloride ions was complicated by several features. Figure 7 shows the angular depen-

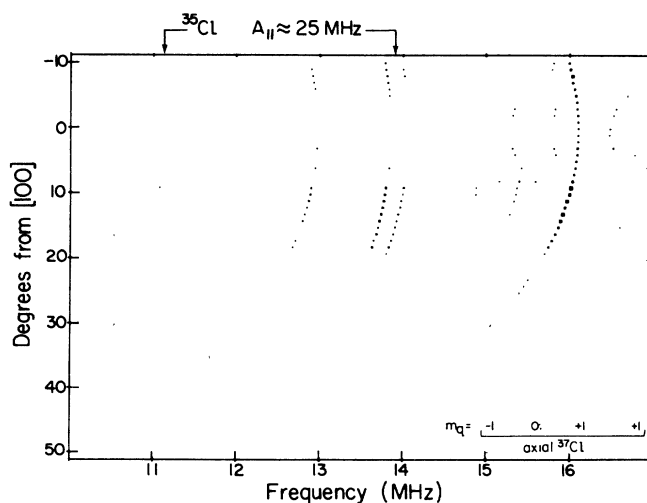


FIG. 7. Angular rotation plot in the xz and yz planes showing the angular dependences for the equatorial chlorine transitions. The dot size is proportional to signal intensity.

dence of a section of the ENDOR spectrum between 9 and 17 MHz for B_0 rotated in the equatorial plane. Double ENDOR experiments for B_0 parallel to z showed that the lines were from the same complexes which gave rise to the other ENDOR lines discussed so far. The relative positions of the ENDOR lines were not consistent with their assignment to rhodium or silver nuclei and were most consistent with an assignment to chloride nuclei. The angular dependences of the lines were consistent with an assignment to first shell chloride ions in the equatorial plane. The intensities of the lines were very dependent on temperature, microwave power, rf modulation frequency, and particularly, on field position. As the magnetic field was shifted by only 1 or 2 mT, new lines would appear and others disappear. It is, at least in part, for this reason that all of the expected equatorial chloride ion's hyperfine, quadrupole, and isotopic transitions were not detected, and regardless of the model used, the ENDOR data could not be fitted exactly.

The transitions, shown in Fig. 7 for B_0 parallel to [100], are in a frequency range which corresponds to a hyperfine value of the order of 20–35 MHz. A more precise value for A_{33} was obtained by iterative simulations of the first-order [100] EPR spectrum for the g_x and g_y components of the primary rhodium complex (Fig. 4). The EPR spectrum was simulated using the experimentally obtained hf data for ^{103}Rh , two axial fourth-shell silver ions, and two axial chloride ions given in Table II, taking into account the relative isotopic abundances and using a Lorentzian linewidth of 2 mT. An excellent fit for the g_x feature was obtained using just these splittings. The largest additional splitting that could be accommodated, assuming the presence of one or two additional chloride ions, was 10 MHz. The symmetric multiplet of the g_y component could only be simulated if two additional spin- $\frac{3}{2}$ splittings with magnitude $\frac{1}{4}$ or $\frac{1}{2}$ of the A_{11} axial chloride splittings were included. A magnitude of 25 MHz gave a suitable spectral width for the g_y multiplet with a minimum EPR line separation of 6 mT. This could be reduced to 3 mT, in good agreement with the experimental spectrum, by including an additional splitting of about 5 MHz from one or two spin- $\frac{3}{2}$ nuclei.

A set of ENDOR lines corresponding to a 25-MHz Cl splitting was indeed observed (marked in Fig. 7). The other ENDOR lines in Fig. 7 must be quadrupole transitions which, of course, do not cause splitting of the EPR spectrum. Thus, for the model in Fig. 2, the 25-MHz parallel splitting, which, according to the EPR simulation must be caused from two equivalent nuclei, can reasonably be assigned to the equatorial chloride ions 4 and 6 along the y axis. Chloride ions 3 and/or 5 could then give rise to the small perpendicular splitting of about 5 MHz with a parallel splitting no larger than 10 MHz. Some of the weak unassigned transitions visible in the angular dependences of Figs. 5 and 7 could possibly arise from the other equatorial chloride ions. However, due to the overlap with other ENDOR lines, a complete analysis was not possible.

The doublet nature of the hyperfine lines from the equatorial chloride ions 4 and 6 is indicative of the presence of two very similar centers. This can be reconciled with the

double ENDOR results, which indicated that all the ENDOR transitions arose from one type of complex if several different rhodium complexes were present which were practically degenerate in their properties along the z axis. The existence of several very similar rhodium centers was also postulated above to explain the anomalous nonaxial fourth-shell silver transitions. Although it is unfortunate that a better analysis of these ENDOR angular dependences was not possible, it should be remarked that ENDOR at least demonstrates clearly that the actual distribution of defect configurations is much more complicated than could have been inferred from the EPR experiments alone.

DISCUSSION

The observation of ^{103}Rh ENDOR transitions confirmed that the primary species in the Rh-AgCl system was a rhodium complex. The observation of only two spin manifolds in the ENDOR spectra further confirmed that $S = \frac{1}{2}$ for the complex. Since g_z was approximately 2, and since the major shf interactions arose from two equivalent chloride ions, we can infer that the unpaired electron had a ground-state wave function with a large rhodium $3d_{z^2}$ contribution.⁹ Based on ligand field arguments, the large $3d_{z^2}$ contribution is indicative of an elongated Rh^{2+} complex.¹² Atomistic calculations,¹³ described further below, also support the picture of an elongated Rh^{2+} complex.

In the silver halide lattice, it is expected that a divalent cation will be charged compensated by the association of a silver ion vacancy. For the primary Rh^{2+} defect in AgCl , the ENDOR analysis showed clearly that the two axial chloride ions (1 and 2) were equivalent. Therefore, the charge compensating Ag^+ vacancy cannot be in a NNN position along the z axis or in a nearest-neighbor (NN) position in the xz or yz planes. The presence of a vacancy in the equatorial plane, however, would account for the concomitant observations of two equivalent axial chloride ions and orthorhombic hf and g matrices which had principal directions along cubic axes. The large degree of orthorhombicity of the rhodium hf matrix suggests that the vacancy was close, either in a NN or NNN position in the equatorial plane. Atomistic simulations¹³ using a wide range of potentials all indicated that the NN configuration was favored by 0.1 to 0.2 eV.¹⁴ We would expect, however, that a NN vacancy would either result in axial g and hyperfine tensors, or would cause an off-axis shift of the principal directions of these tensors, as was seen for Ni^{1+} nearest neighbor in AgCl .¹⁵ Such a shift was not observed within the experimental accuracy of $\pm 4^\circ$. Thus, the NN vacancy configuration is ruled out.

The assignment of an equatorial NNN vacancy is consistent with the dynamic changes observed in the EPR spectrum. The temperature behavior described above clearly indicates that the primary complex undergoes a dynamic distortion as the temperature is raised. The near equality of the g_x value of the LT form with the g_{\parallel} value of the HT form, and the fact that g_{\perp} for the HT form was the average of g_y and g_z for the LT form, suggests that the

distortion occurs about g_x in the yz plane. The possibility that the observed averaging behavior occurred as a result of vacancy motion can be ruled out since ionic motion was frozen out at the temperatures at which averaging began to take place. The averaging behavior can, however, be explained by a two-dimensional dynamic distortion, in which the presence of the vacancy raises the configuration energy for elongation along the x axis so that averaging only occurs in the yz plane. The averaging can be described as a hopping of the axis of elongation of the complex between the y and z axes. A similar motion was observed for the Sn^+ next-nearest-neighbor vacancy complex in KCl (Ref. 16) and for the $(\text{AgBrCl}_5)^{4-}$ complex in Br^- -doped AgCl .¹⁷ As the temperature was raised still further, an isotropic line corresponding to a three-dimensional distortion was observed. This could be the result of overcoming the barrier for distortion along the x axis and/or thermally stimulated vacancy motion.

As mentioned above, at high rhodium dopant levels complete spectral averaging occurred at higher temperatures than at low dopant levels. This can reasonably be attributed to the presence of both isolated rhodium-vacancy complexes and complexes perturbed by distant defects, as detected in the ENDOR experiments described above. The proximity of such defects might be expected to affect the barrier heights between the three distorted complex configurations. The high rhodium dopant levels used for the "heavily doped" crystals makes it likely that the perturbing defects were other rhodium ions or clusters, especially given the propensity for rhodium ions to aggregate in the silver halides.¹⁸

The assignment of the vacancy to the x -axis NNN position is also supported by the EPR simulations which showed that the largest shf interactions of the equatorial chloride ions arose from two chloride ions along the y axis and that these ions were equivalent or nearly equivalent.

The $2+$ charge state of the rhodium complex is supported by an estimate of the quadrupole interactions of the axial chloride ions. The quadrupole interaction constant q is related to the electric field gradient at the nucleus by

$$q = \frac{eQ}{4I(2I-1)} \left[\sum_i \frac{2q_i}{r_i^3} (1 - \gamma_{\infty}) + f_p q_p \right], \quad (7)$$

where the field gradient is made up of contributions from point charges and from unpaired electron density in p orbitals. Contributions from covalent bonding of inner-shell rhodium electrons were ignored. $(1 - \gamma_{\infty})$ is the Sternheimer antishielding factor and q_p is 80 MHz for ^{35}Cl .¹⁹ The contribution to q from the net excess charge at the rhodium nucleus was -1.24 MHz, from the negative charge due to the silver ion vacancy in a NNN position, $+0.035$ MHz, and from the unpaired electron spin density at the axial chloride ions, calculated from the measured anisotropic hyperfine constant, $+1.05$ MHz. The total calculated q of -0.16 MHz compares favorably with the measured value of -0.40 MHz (Table II). The discrepancy is easily within the uncertainties of the approximation. The discrepancy is larger by a factor of 2 for an equatorial NN vacancy. A similar calculation ruled out the charge state of Rh^0 ($q_{\text{calc}} = +2.3$ MHz). Likewise, the presence of a vacancy along the complex z

axis could be excluded.

An estimate of the measured shf constant for the axial chloride ions was done using the usual one-particle approach:²⁰

$$a = \frac{2}{3} C |\psi(0)|^2, \quad (8)$$

$$b = \frac{\mu_0}{8\pi} C \int \frac{3z^2 - r^2}{r^5} |\psi(r)|^2 dV,$$

where C represents $g_e \mu_B g_I \mu_N$. ψ is the envelope wave function of the rhodium complex. If the rhodium $3d_{z^2}$ orbital is used as an envelope function and orthogonalized to the Cl^- cores, 30% of the observed isotropic shf constant and only 7% of the anisotropic shf constant can be accounted for. The classical dipole-dipole interaction is only 0.37 MHz for the undistorted lattice. In estimating the shf constants, we used the analytical Hartree-Fock orbitals for the free ions Cl^- , Ag^+ , and Rh^+ given by Clementi and Roetti.²¹ Rh^+ wave functions were used because of a lack of wave functions for Rh^{2+} . The results obtained should be relevant, however, since the discrepancies described above would be exaggerated by the more contracted envelope wave function of Rh^{2+} .

As a result of the excess positive charge at the Rh^{2+} nucleus, one might expect an inward relaxation of the first ligand shell of chloride ions, a distortion that would improve the agreement between measured and calculated shf parameters.¹⁴ It is necessary, however, to also consider the effects of the nonspherical distribution of d -electron density. Preliminary atomistic simulations that took into account the nonspherical electronic distribution found that while the equatorial chloride ions showed a tendency to relax inwards by about 5%, the inward relaxation of the axial chloride ions was cancelled by the outward repulsions due to the unpaired electron in the $3d_{z^2}$ orbital.¹⁴ Thus, the complex was predicted to be elongated along z , in agreement with experiment, and lattice relaxation cannot account for the large discrepancy between measured and calculated axial Cl^- shf parameters.

Taking the wave function used for the $\text{Cl}^- \text{Rh}^{2+} \text{Cl}^-$ subsystem and orthogonalizing it to the cores of the fourth-shell silver ions, we obtain shf interactions which are 6 orders of magnitude too small to account for the observed splittings. If we consider a transferred shf interaction, that is, the interaction which results from the overlap of the axial chloride ions and the fourth-shell silvers, a and b are given approximately by²⁰

$$a = \left(\frac{2}{3} \mu_0 C\right) f_s \langle \psi_{\text{Cl}_{3z^-}} | \psi_{\text{Ag}_{4z^+}} \rangle^2 | \psi_{\text{Ag}_{4z^+}}(0) |^2, \quad (9)$$

$$b = \left[\frac{\mu_0}{8\pi} C \right] \left(\sqrt{f_p} \langle \psi_{\text{Cl}_{3p\sigma^-}} | \psi_{\text{Ag}_{4p\sigma^-}} \rangle + \sqrt{f_s} \langle \psi_{\text{Cl}_{3z^-}} | \psi_{\text{Ag}_{4p\sigma^+}} \rangle \right)^2 \frac{1}{r^3} | \psi_{\text{Ag}_{4p}} |^2 dV,$$

where the terms f_s and f_p are the ligand spin densities calculated from the experimental shf constants. For the transferred interaction, the calculated anisotropic interaction is too small by a factor of 0.63. Once again, the discrepancy cannot be ascribed to lattice relaxation since atomistic calculations indicated that the axial fourth-shell

silver ions moved inwards by less than 1%.¹⁴

The discrepancies between the calculated and experimental shf data for the axial chloride and fourth-shell silver ions indicate that bonding in the rhodium defect cluster cannot be treated as purely ionic. This suggests that bonding in the rhodium clusters and the surrounding AgCl lattice has some covalent character.²²

It is interesting to note that a major effect of the NNN silver ion vacancy in the rhodium-vacancy complex was to reduce electron density along the vacancy axis. This can be seen from a comparison of the equatorial Cl^- shf parameters expected for a complex with no perturbing vacancy with the shf values reported here for the perturbed complex. For an unperturbed complex, assuming a $3d_{z^2}$ envelope function, the unpaired electron spin density and the shf parameters for each of the equatorial Cl^- ions should be $\frac{1}{4}$ the value for each of the axial Cl^- ions. For the perturbed rhodium complex, spectral simulations showed that along the rhodium-vacancy axis Cl^- shf values were less than $\frac{1}{8}$ of axial Cl^- shf values. Conversely, for equatorial Cl^- ions 4 and 6, not on the rhodium-vacancy axis, the estimated shf parameters were about 30% those of the axial Cl^- ions. This larger value reflects, at least in part, the inward relaxation of the equatorial Cl^- ions which were calculated by atomistic simulation methods.¹⁴ The effect of the vacancy in reducing electron density also appeared in the dynamic behavior of the complex, where it was observed that the configuration with " d_{z^2} " along the x axis of the complex was energetically unfavorable.

CONCLUSIONS

It was shown that the primary rhodium complex in AgCl was an orthorhombic Rh^{2+} complex elongated along a $[100]$ crystal axis with a silver ion vacancy in a NNN position in the plane perpendicular to the elongation axis. The presence of the vacancy reduced electron density along the rhodium-vacancy axis. The model deduced provided an explanation for the dynamic behavior of the complex observed above 110 K.

The measured superhyperfine interactions for the lattice ions along the rhodium complex elongation axis were larger than those calculated considering only ionic interactions. Atomistic calculations showed that the discrepancies could not be attributed to lattice relaxation around the impurity ion. Thus, it is suggested that a degree of covalency exists in the $[\text{RhCl}_6\text{Ag}_2]^0$ cluster and/or the host lattice.

ACKNOWLEDGMENTS

We gratefully acknowledge many helpful discussions with Dr. R. S. Eachus and Dr. R. C. Baetzold. We would also like to thank Dr. R. H. Nuttall for development of the spectral simulation programs used in this study. Finally, we gratefully acknowledge helpful discussions with Professor D. Schoemaker, who brought this problem to our attention, suggesting the correlation between the dynamic behavior of the rhodium complex and its structure.

- ¹R. S. Eachus and M. T. Olm, *Radiat. Eff.* **73**, 69 (1983).
- ²D. A. Corrigan, R. S. Eachus, R. E. Graves, and M. T. Olm, *J. Chem. Phys.* **70**, 5676 (1979).
- ³R. S. Eachus, R. E. Graves, and M. T. Olm, *J. Chem. Phys.* **69**, 4580 (1978).
- ⁴R. S. Eachus and R. E. Graves, *J. Chem. Phys.* **61**, 2860 (1974).
- ⁵J. Wilkens, D. P. DeGraag, and J. N. Helle, *Phys. Lett.* **19**, 178 (1965).
- ⁶J. R. Shock and M. T. Rogers, *J. Chem. Phys.* **62**, 2640 (1975).
- ⁷J. R. Niklas, *Habilitationsschrift*, Universitat Gesamthochschule, Paderborn, 1983.
- ⁸H. Seidel, *Habilitationsschrift*, Technischen Hochschule, Stuttgart, 1966.
- ⁹A. Abragam and B. Bleaney, *Electron Paramagnetic Resonance of Transition Ions* (Clarendon, Oxford, 1970).
- ¹⁰T. E. Feuchtwang, *Phys. Rev.* **126**, 1628 (1962).
- ¹¹J. R. Niklas and J. M. Spaeth, *Phys. Status Solidi (b)* **101**, 221 (1980).
- ¹²C. J. Ballhausen, *Introduction to Ligand Field Theory* (McGraw-Hill, New York, 1962).
- ¹³C. R. A. Catlow, M. Dixon, and W. C. Mackrodt, *Computer Simulations of Solids* (Springer-Verlag, Berlin, 1982).
- ¹⁴R. C. Baetzold (unpublished).
- ¹⁵G. E. Holmberg and L. M. Slifkin, *J. Phys. C* **10**, 2897 (1977).
- ¹⁶C. J. Delbecq, R. Hartford, D. Schoemaker, and P. H. Yuster, *Phys. Rev. B* **13**, 3631 (1976).
- ¹⁷M. Yamaga, Y. Hayashi, and H. Yosioka, *J. Phys. Soc. Jpn.* **44**, 154 (1978).
- ¹⁸R. S. Eachus and M. T. Olm (unpublished).
- ¹⁹C. P. Slichter, *Principles of Magnetic Resonance* (Springer-Verlag, New York, 1980), p. 292.
- ²⁰J. M. Spaeth and H. Seidel, *Phys. Status Solidi (b)* **46**, 323 (1971).
- ²¹E. Clementi and C. Roetti, *At. Data Nucl. Data Tables* **14**, 177 (1974).
- ²²W. Andreoni and K. Maschke, *Solid State Ionics* **9-10**, 1389 (1983).